Journal of Thermal Analysis and Calorimetry (2019) 137:1021–1030
https://doi.org/10.1007/s10973-018-07995-8

Kinetic modeling for thermal hazard of 2,2′-azobis (2-methylpropionamide) dihydrochloride using calorimetric approach and simulation

Chen-Rui Cao[1] · Chi-Min Shu[2]

Received: 6 August 2018 / Accepted: 23 December 2018 / Published online: 3 January 2019

Abstract

Azo compounds are usually used as initiators and blowing agents. They are also typically self-reactive materials capable of undergoing a runaway reaction during storage or transportation, which can cause serious fires and explosions. To prevent the thermal hazard of azos occurring in a real process, transportation, or storage, azo initiator 2,2′-azobis (2-methylpropionamide) dihydrochloride (AIBA), which has few studies on relevant research in thermal safety, was selected to be investigated. First, the features of thermal decomposition under non-isothermal condition of AIBA were attained through differential scanning calorimetry and simultaneous thermal analysis. Second, the collected data were substituted into mathematical analyzer to evaluate the basic thermal hazard for AIBA. In addition, based on Semenov theoretical model and thermokinetic parameters, the critical ignition temperature (T_{CI}) was extrapolated for consideration of surroundings temperature under specific cooling system (T_S). The results provided process control data and the consequences of thermal runaway for AIBA. In addition, the related numerical methods for prevention of thermal runaway reaction could be calculated during process deviation. Therefore, the assessment conclusions also showed that process parameters must be measured and controlled strictly to generate the desired reaction. The results showed that the various T_{CI} were all less than 70 °C. Therefore, it is essential to avoid a temperature beyond the T_{CI} or cooling system failure.

Keywords Azo compounds · 2,2′-Azobis (2-methylpropionamide) dihydrochloride (AIBA) · Differential scanning calorimetry · Semenov theoretical models · Critical ignition temperature (T_{CI}) · Numerical methods

List of symbols

R	Gas constant/8.31415 J K^{-1} mol^{-1}
A	Pre-exponential factor of Arrhenius equation (min^{-1})
$A(\alpha)$	Pre-exponential factor at conversion (min^{-1})
$A'(\alpha)$	Amended pre-exponential factor by a product of $A(\alpha)$ and $f(\alpha)$ (min^{-1})
C_o	Original concentration of the material (g cm^{-3})
C	Concentration of the material (g $cm^{-3)}$
C_p	Specific heat of material (J g^{-1} K^{-1})
E_a	Apparent activation energy (kJ mol^{-1})
$E(\alpha)$	Apparent activation energy factor at conversion (kJ mol^{-1})
h	Heat exchange capability index of the cooling system (kJ m^{-2} K^{-1} min^{-1})
k_0	Reaction rate constant (s^{-1})
n	Reaction order (dimensionless)
m	Mass of material (g)
ΔH_d	Heat of decomposition (J g^{-1})
ΔH_t	Heat of decomposition at time (J g^{-1})
ΔH_{total}	Total heat of decomposition (J g^{-1})
r	Reaction rate (s^{-1})
q_g	Heat production rate (kJ min^{-1})
q_r	Heat removal rate (kJ min^{-1})
q_{r1}	Heat removal rate by high cooling medium (kJ min^{-1})
q_{r2}	Heat removal rate by cooling system (kJ min^{-1})
q_{r3}	Heat removal rate by low cooling system (kJ min^{-1})
S	Effective heat exchange area (m^2)

✉ Chi-Min Shu
shucm@yuntech.edu.tw

[1] Graduate School of Engineering Science and Technology, National Yunlin University of Science and Technology (YunTech), 123, University Rd., Sec. 3, Douliou 64002, Yunlin, Taiwan, ROC

[2] Department of Safety, Health, and Environment Engineering, YunTech, 123, University Rd., Sec. 3, Douliou 64002, Yunlin, Taiwan, ROC

V	Volume of process instruments (m^3)
T	Process temperature (K)
T_0	Apparent exothermic temperature (K)
T_P	Temperature at the maximum heat release in reaction (K)
T_S	Surrounding temperature under cooling system (K)
t	Reaction time (min)
T_{CI}	Critical ignition or extinction temperature (K)
T_{CE}	Critical extinguishing temperature (K)
T_{SE}	Stable point of extinguishing temperature (K)
T_{SI}	Stable point of ignition temperature (K)
T_{SL}	Stable point at lower temperature (K)
T_{SH}	Stable point at higher temperature (K)
T_M	Cutoff point between curves q_g and q_r at the highest and lowest cooling efficient system (K)
X_A	Fractional conversion (dimensionless)
α	Degree of conversion (dimensionless)

Introduction

Azo compounds (azos), materials that easily show unstable performance, are commonly used in radical polymerization in solution. If the temperature of the surrounding environment or process is under improper control, thermal decomposition, generating heat release, may even court a thermal explosion [1].

In the United Nations (UN) classification of dangerous goods, the azos stand as a class 4.1 hazardous category of material. Fire and Disaster Management Agency (FDMA) of Japan defined the azos as the 5th category of dangerous substances, which include diazos, organic peroxides, esters, nitrous, and the mixture containing one of the above substances [1–4]. Thus, the azo compound has a certain self-reactive trait.

R–N=N–R is a synthesis reaction formula of azo compound, wherein R is an aliphatic hydrocarbon group or an aromatic hydrocarbon group; two R groups may be the same or different. Aliphatic azos are made from the corresponding hydrazine through oxidation or dehydrogenation reaction [3–7]. Aromatic azos, which are generally prepared by the coupling reaction of diazo compound, are mainly used for dyes, and aliphatic azos are used more in the polymerization initiator. The azo initiator, which is selected to research, 2,2′-azobis (2-methylpropionamide) dihydrochloride (AIBA), is widely used in chemical processes. Although there are a series of studies on the individual and multiple thermal hazards of azos [5–9], there is less research on AIBA in the past literature. Most of the research focused on thermal hazard by single calorimetry technique or less on numerical analysis of data under the conditions of processing, storage, or transportation of AIBA.

In essence, azos do not need oxygen in the air or water vapor but can react by themselves, and are often accompanied by an exothermic and gas-product formation. Chemical stability of such self-reactive materials is poor. The slow decomposition will indiscernibly occur even at ambient temperature.

During reaction, storage, or transportation, when the heat production rate (Q_g) surpasses the heat removal rate (Q_r), the heat released in the reaction process leads to an increment in temperature (T). As the process temperature reaches the apparent exothermic onset temperature (T_0), the system may eventually cause the reaction to gradually become unbalanced, and a runaway reaction may even be started. At this instant, if the heat cannot properly be removed, heat accumulation will cause a temperature rise, increasing the progress of reaction and leading the reaction system to combustion, bursting, or even explosion [10–12].

We used differential scanning calorimetry (DSC) combined with thermogravimetric analysis (TG) to determine the thermal runaway reaction of AIBA by several heating rates (β). Based on instrument data, numerical methods were the primary technique for further analysis on reaction kinetic of AIBA [13–17]. Mathematical models [18–21] bring into kinetic assessment operation for quantification and calculation, as well as to establish a specification of assessment for development and preserve the process into stable state. The estimate model was employed to assess thermokinetic parameters, such as apparent exothermic temperature (T_0), reaction order (n), temperature at the maximum heat release in reaction (T_p), heat of decomposition (ΔH_d), pre-exponential factor (A), and apparent activation energy (E_a). Above-obtained data were applied to classify and construe exothermic mode of AIBA under large scale, and corresponding thermal safety measures can also be analyzed. The mathematical approach combining thermal hazard responses evaluation is a critical basis for the rationality of thermokinetic parameters. To achieve this objective, we used two kinds of isoconversional methods as a preliminary estimate of the thermal hazard parameters and imported two linear fitting methods to calculate the required values that are further required for the process amplification method. Scale-up simulation was implemented by Semenov model [22], which can be applied in real process situation, transportation, or storage conditions.

Experimental and methods

Thermokinetic parameters of AIBA reaction

The basic thermal hazard characteristics of 98 mass% AIBA were determined by DSC temperature screening experiments with a software setting on a Mettler TA8000 system subjoined with a DSC 821^e measuring cell [23, 24]. Thermogravimetry, purchased from Hitachi STA 7200RV (simultaneous thermal analysis), was utilized to analyze the alterations of mass loss and thermal degradation behavior for AIBA. Five heating rates of 0.5, 1.0, 2.0, 4.0, and 8.0 °C min^{-1} were applied in DSC and STA [25].

For acquiring appropriate values for the correctness of the subsequent calculation, we combined the differential isoconversional of Friedman, and Flynn–Wall–Ozawa methods with linear fitting of ASTM E698-11 and Kissinger methods for preliminary determining rudimentary thermokinetic parameters. The calculated data can be used as the basis for the process amplification simulation.

Isoconversional differential method–Friedman method

The Friedman method uses a differential isoconversional model, which is derived from the Arrhenius equation, to determine thermokinetic parameters [26]. The data measured by calorimetry can be determined from natural logarithmic transformation on conversion rate $(\mathrm{d}\alpha/\mathrm{d}t)$, externalized for formula on reciprocal of corresponding reaction conversion rate $(\alpha)t$ specific absolute temperature [27]:

$$\ln\left(\frac{\mathrm{d}\alpha}{\mathrm{d}t}\right) = \ln(A(\alpha)f(\alpha))\exp\left(-\frac{E(\alpha)}{RT(t)}\right) \tag{1}$$

$$t_a = \int_0^t \mathrm{d}t = \int_{\alpha_0}^{\alpha} \frac{\mathrm{d}\alpha}{A'(\alpha)\exp\left(-\frac{E(\alpha)}{RT(t)}\right)} \tag{2}$$

In Eq. (1), $E(\alpha)$ and $A(\alpha)$ are apparent activation energy and frequency factor at conversion α; $A'(\alpha)$ is an amended pre-exponential factor by a product of $A(\alpha)$ and $f(\alpha)$. $f(\alpha)$ is reaction equation. The reaction equation will have different expression patterns depending on the reaction mode of the sample itself, but the method does not need to consider the form of the reaction, so $f(\alpha)$ can be expressed as a constant. The calculating method of E_a is indicated as relational equation between parameters of $-E(\alpha)\ R^{-1}$ in slope and $\ln(A(\alpha)f(\alpha))$ in intercept. The coordinate of x and y axes is characterized by ln $(\mathrm{d}\alpha/\mathrm{d}t)$ and $T(t)^{-1}$.

Isoconversional integration–Flynn–Wall–Ozawa method

Flynn–Wall–Ozawa method avoids the possible negligence produced from diverse assumptions concerning kinetic form, which can be expressed as below [28]:

$$\ln(\beta) = -1.0516\left(\frac{E_a}{RT}\right) + \text{constant} \tag{3}$$

If the effects of different heating rates are taken into account, Eq. (3) can be rewritten as Eq. (4):

$$\begin{aligned}\ln(\beta_1) + 1.0516\frac{E_{ai}}{RT_{a1}} &= \ln(\beta_2) + 1.0516\frac{E_{ai}}{RT_{a2}} \\ &= \ln(\beta_3) + 1.0516\frac{E_{ai}}{RT_{a3}} = \cdots\end{aligned} \tag{4}$$

The slope E_α can be determined by plotting with ln (β) and T^{-1}. Isoconversional methods have a prominent advantage over non-isoconversional methods. The results, in a wide range of applications actual sample temperatures, may deviate from preset non-isothermal or isothermal methods. This is due to the thermal effect that induces sample self-heating [28]. The method is better suited for a differential type instrument, such as heat-flow data by DSC. The method does not need to consider the models and process of reaction which can be made a preliminary analysis to verify the apparent activation energy [28].

ASTM E698-11 model

The suitability and application of the linear fitting method have been confirmed in several papers for its methodological strength. Compared to the isoconversional method, linear fitting method is applicable for known reaction modes such as nth reaction, or where substances are less complex in the reaction stage. If the reactions are correctly matched, the conditions of the fitting and the result can be relied upon. In this study, the Kissinger method and ASTM E698-11 are deemed suitable for use.

The ASTM E698-11 method can be written in the following form [29]:

$$E_a = \left(-\frac{2.303R}{D}\right)\left[\frac{\mathrm{d}(\log\beta)}{\mathrm{d}\left(\frac{1}{T_P}\right)}\right] \tag{5}$$

$$D = \frac{\mathrm{d}\ln[p(x)]}{\mathrm{d}x} = \frac{\mathrm{d}\ln(x+2)x\exp(x)}{\mathrm{d}x}, \quad \text{where } x = \frac{E_a}{RT_P} \tag{6}$$

$$A = \frac{E_a\beta}{RT_P^2}\exp\left(\frac{E_a}{RT_P}\right) \tag{7}$$

where α is the conversion of the AIBA groups and A is the rate constant. The values of $\ln(\beta/T^2)$ and T^{-1} in the plot can render the slope = $-E_\alpha/(RT)$.

Kissinger method

The A and E_α can be calculated from drawing the y axes of $\ln[\beta/T_p^2]$ and x axes of $1/T_p$ [30]:

$$\ln\left(\frac{\beta}{T_p^2}\right) = \ln\left(\frac{AR}{E_a}\right) - \frac{E_a}{RT_p} \tag{8}$$

Calculating relative speed and convenience of the essential parameters are benefits of the linear fitting method, such as ASTM E698-11 and Kissinger methods which were applied in this study. Linear fitting method is usually based on the Arrhenius model, which involves a certain range of heating rates, generally set as 1–10 °C min^{-1} and assuming a first-order reaction in applied elementary chemical processes, such as decomposition, catalysis, and degradation [30].

Nonlinear fitting method

To clarify the thermokinetics for AIBA, a nonlinear fitting method was applied for DSC thermal curve data treatment [14, 31, 32]. The nonlinear fitting method assumes that the conversion degrees are reflected in variables of systematic status. This approach not only facilitates to establish a more detailed reaction mechanism, but is also consistent with the actual situation and some experimentally obtained overall responses. In addition, the condition occurs when investigating reactions in other self-reactive substances and secondary reactions with more than two stages initiated at elevated temperatures under accidental environments. The nonlinear fitting method can characterize multiple phase reactions that may contain several independent, parallel, and continuous stages. The nth reaction rate models used in this study are demonstrated in Eqs. (9) and (10) [31, 32]:

Simple single-stage reaction A → B:

$$r = \frac{d\alpha}{dt} = k_o e^{-\frac{E_a}{RT}} f(\alpha) \times \begin{cases} \text{For } n\text{th-order model}: f(\alpha) = (1-\alpha)^n & (9) \\ \text{For autocatalysis model}: f(\alpha) = (1-\alpha)^{n_1}(\alpha^{n_2} + \eta) & (10) \end{cases}$$

where k_o denotes the pre-exponential factor of reaction of the nth stage, respectively. R is the gas constant (R = 8.314 J mol^{-1} K^{-1}), α is the degree of conversion (0–1), and η is the autocatalytic constant.

Process amplification with simulation method and critical condition calculation

Scale-up method is based upon the assumption that (1) the temperature in the system is uniform, (2) there is no temperature gradient, and (3) the temperature of the system is greater than that of the environment. The heat exchange between the system and the environment is concentrated on the surface of the system [33]. This approach not only builds up a more detailed reaction mechanism, but is also in line with the actual situation, and some overall responses, such as heat generation in real process, can be obtained [34]. The fractional conversion of concentration rate X_A can be converted to Eqs. (11) and (12) [22, 35]:

$$X_A = \frac{\Delta H_t}{\Delta H_{total}} = \frac{mC_p(T - T_o)}{mC_p(T_p - T_o)} = mC_p\frac{(T - T_o)}{(T_p - T_o)} \tag{11}$$

$$C = C_o(1 - X_A) = C_o\frac{(Tp - T)}{(Tp - T_o)} = C_o\frac{(Tp - T)}{\Delta Tp} \tag{12}$$

where C is concentration of reactants, C_o is initial concentration, $\triangle H_t$ is total heat released by decomposition at time, $\triangle H_{total}$ is total heat of whole reaction, m is mass of reactants, and C_P is specific heat of reactants of interest [35].

The equation of reaction rate (r) can be exemplified as Eq. (13) [36]:

$$-r = \frac{-dC}{dt} = kC^n \tag{13}$$

where k is rate constant, t is a specific period in the chemical process, and n is reaction order.

Substituting and combining Eq. (12) with Eq. (13) and the Arrhenius equation:

$$k = C_o^{n-1}A\exp\left(-\frac{E_\alpha}{RT}\right) = \left(\frac{dT}{dt}\right)\left[\frac{\Delta T_p}{(T_p - T)}\right]^n \Delta T_p \tag{14}$$

Taking the transformation on natural logarithms on Eq. (14) renders Eq. (15) on the following information:

$$\ln k = \ln\left\{\left(\frac{dT}{dt}\right)\left[\frac{\Delta T_p}{(T_p - T)}\right]^n \Delta T_p\right\} = \ln\left(C_o^{n-1}A\right) - \frac{E_a}{RT} \tag{15}$$

The dT/dt by adiabatic condition is the magnitude of the temperature rise within the reaction. Amplification model demonstrates heat production rate (q_g) composed with volume of reactive material (V), $-r$, and $\triangle H_{total}$. q_g is indicated as Eq. (16):

$$q_g = \Delta H_{total} V(-r) \tag{16}$$

Replacing Eq. (13) into Eq. (16), q_g can be rewritten as Eq. (17):

$$q_g = \Delta H_{total} V A C^n \exp\left(-\frac{E_a}{RT}\right) \quad (17)$$

The heat reduction rate (q_r) caused by cooling system is denoted as Eq. (18):

$$q_r = hS(T - T_s) \quad (18)$$

where h can be expressed as heat transfer capacity of cooling system, S is total contact surface area for heat exchange, and T_S is ambient temperature under current system.

Derived from Eqs. (17) and (18), the thermal balance of system $q_g - q_r$ can be represented as Eq. (19):

$$\rho V C_P \left(\frac{dT}{dt}\right) = q_g - q_r \quad (19)$$

where ρ is density of reactants.

From Eqs. (17) to (19), the thermal change in system can be annotated as Eq. (20):

$$\rho V C_P \left(\frac{dT}{dt}\right) = \Delta H_{total} V A C^n \exp\left(-\frac{E_a}{RT}\right) - hS(T - T_s) \quad (20)$$

The reaction order n obtained by this study is 1. Therefore, replacing Eq. (17) into Eq. (20) with $n = 1$, Eq. (20) can be rewritten as Eq. (21):

$$\rho V C_P \left(\frac{dT}{dt}\right) = \Delta H_{total} V A C_o \left[\frac{(T_P - T)}{(T_P - T_o)}\right] \exp\left(-\frac{E_a}{RT_c}\right) = hS(T_C - T_S) \quad (21)$$

Whether the reaction is in equilibrium under steady state can be obtained by Eqs. (22) and (23) [22]:

$$q_g|_{T=T_c} = q_r|_{T=T_c} \quad (22)$$

$$\left.\frac{dq_g}{dT}\right|_{T=T_c} = \left.\frac{dq_r}{dT}\right|_{T=T_c} \quad (23)$$

where T_c is the critical temperature.

When the q_g subtracted q_r is a negative value, $(dT/dt) > 0$. The cooling system is unable to process the heat generated in the system. As heat continues to accumulate in the system, it is eventually evolving into runaway. With above condition, Eq. (21) can be rewritten as Eq. (24):

$$\Delta H_{total} V A C_o \left[\frac{(T_P - T_C)}{(T_P - T_o)}\right] \exp\left(-\frac{E_a}{RT_c}\right) = hS(T_C - T_S) \quad (24)$$

Combining Eqs. (22) and (23), applicable conditions of heat transfer efficiency hS can be calculated:

$$hS = \frac{\Delta H_{total} V A C_o \exp\left(\frac{-E_a}{RT_c}\right)\left[-1 + \frac{E_a(T_p - T_c)}{RT_c^2}\right]}{(T_p - T_o)} \quad (25)$$

Results and discussion

Thermokinetic parameters of AIBA reaction

Thermogravimetry can be used to examine the association between temperature and mass loss for the decomposition or combustion reaction. Therefore, the thermal stability of chemicals can be evaluated in a heating system. Figure 1 shows the mass loss versus time diagram of AIBA in N_2 atmosphere at different heating rates, 0.5, 1.0, 2.0, 4.0, and 8.0 °C min^{-1}, by TG test. The time of thermal degradation is lessened with temperature increase, and even the time of thermal degradation of AIBA is less than 8.0 h at low heating rate (0.50 °C min^{-1}), which is defined that the base of AIBA is thermally sensitive material. Moreover, when heating exceeds 4.0 °C min^{-1}, the thermal degradation of AIBA becomes quite violent. Therefore, during the storage or transportation, AIBA should remain at lower temperature to avoid aging or thermal hazard from occurring.

Figure 2 demonstrates the mass loss rate against time diagram of AIBA by TG tests. It can be seen that the AIBA has two mass loss stages and also stands for a severe decomposition reaction. The response amplitude of first stage is a minor effect in the overall reaction, as shown in Fig. 1. We regard the second stage as the main reaction to obtain the thermokinetic parameter under the nonlinear fitting method, and simulation result is well matched with experimental data. It is reasonable to treat the second-stage reaction as the main reaction and the basis for the subsequent process amplification calculation.

By the arithmetic results of isoconversional method, the conversion of reaction progress α is in the range of values on 0–1 and presented in Figs. 3 and 4. As the reaction proceeds, AIBA has a short prompt reduction of E_a. The value of E_α remains without much change, and then, it is

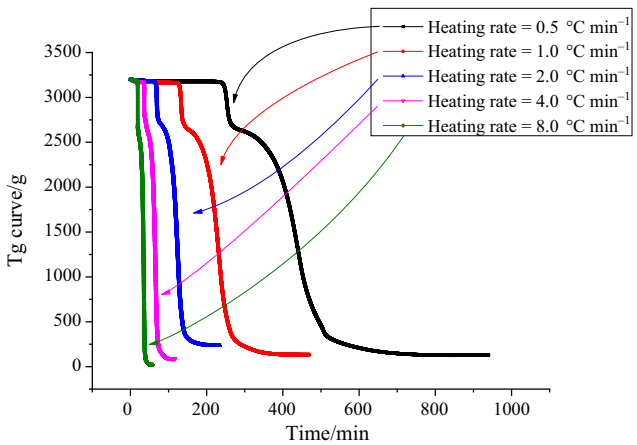

Fig. 1 TG thermal curves of AIBA at of 0.5, 1.0, 2.0, 4.0, and 8.0 °C min^{-1}

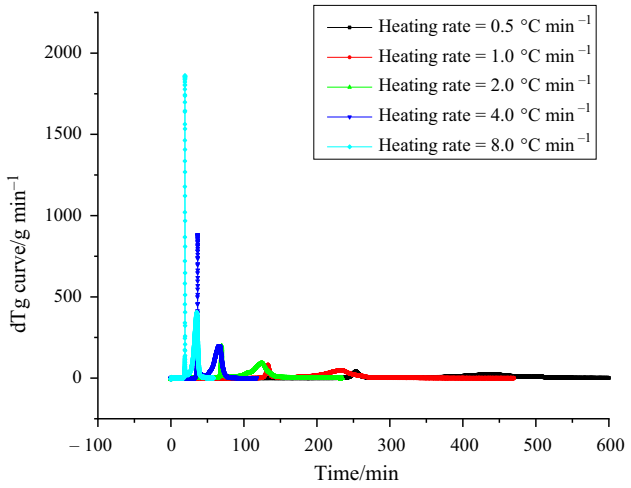

Fig. 2 dTg thermal curves of AIBA at of 0.5, 1.0, 2.0, 4.0, and 8.0 °C min^{-1}

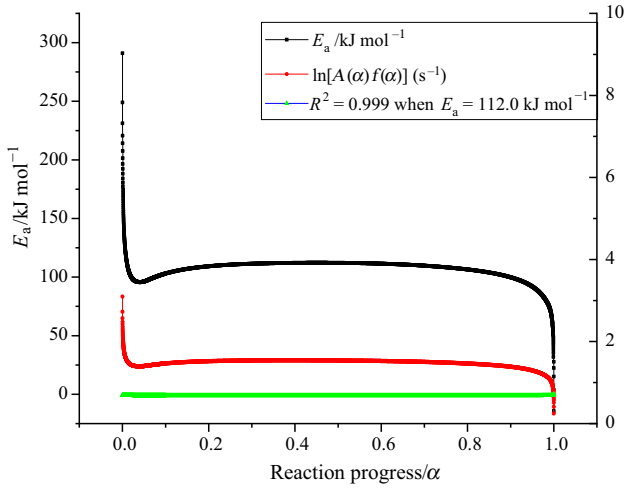

Fig. 3 Determination of the apparent activation energy of the decomposition of 98 mass% AIBA with the Friedman thermokinetic equation

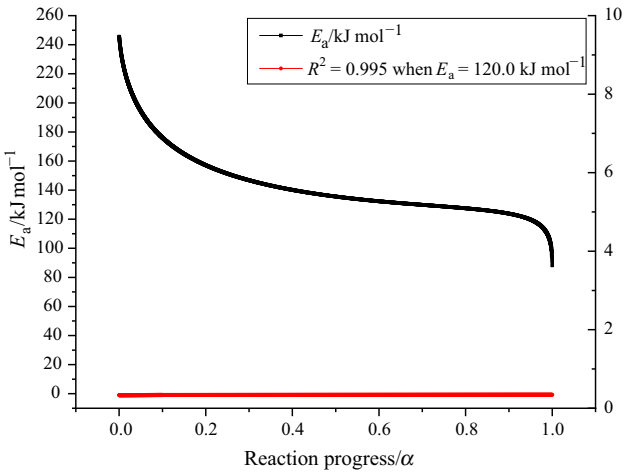

Fig. 4 Determination of the apparent activation energy of the decomposition of 98 mass% AIBA with the Flynn–Wall–Ozawa thermokinetic equation

Table 1 Non-isothermal data by DSC tests for 98 mass% AIBA at 0.5, 1.0, 2.0, 4.0, and 8.0 °C min^{-1}

β/°C min^{-1}	T_0/°C	T_p/°C	ΔH_d/J g^{-1}
AIBA			
0.5	93.0	99.7	875.0
1.0	101.0	105.5	837.0
2.0	107.0	111.4	887.0
4.0	113.0	117.6	1097.0
8.0	121.0	126.1	1185.0

Table 2 Calculated results of E_a value by four methods

Method	E_a/kJ mol^{-1}
Friedman	100–112
Flynn–Wall–Ozawa	99–200
ASTM E698-11	120
Kissinger	125

reduced at the end of reaction. The minimum value of E_α occurs at the end of the reaction. The value of E_a varies greatly to the beginning and end of the reaction. The values of E_a provided by reaction process are remaining stable. It can be inferred that AIBA is basically a relatively simple model on decomposition reaction, approximated as an *n*th order reaction.

For AIBA, the ranges of E_a from two isoconversional methods are 100.0–112.0 and 99.0–200.0 kJ mol^{-1}, which can be obtained from the data shown in Table 1. Table 2 shows the calculated results from four methods, which can be compared. Among the E_a values, the result from Friedman model is different from the other three models. Even experiments conducted under the same setting conditions cannot be confirmed by the consistency of data retention. A single scanning may cause an offset in instruments. However, the deviation of the calculations and experimentation was greatly reduced by Friedman model, which did not require an accurate understanding of reaction pathway. The results of Flynn–Wall–Ozawa are more suitable for AIBA. Combining the results of ASTM E698 on Fig. 5 and Kissinger methods on Fig. 6, it can be determined that E_a = 125.0 kJ mol^{-1} instead of a range of values.

Figures 7 and 8 show heat production versus time for the experiments and simulations. The simulation results

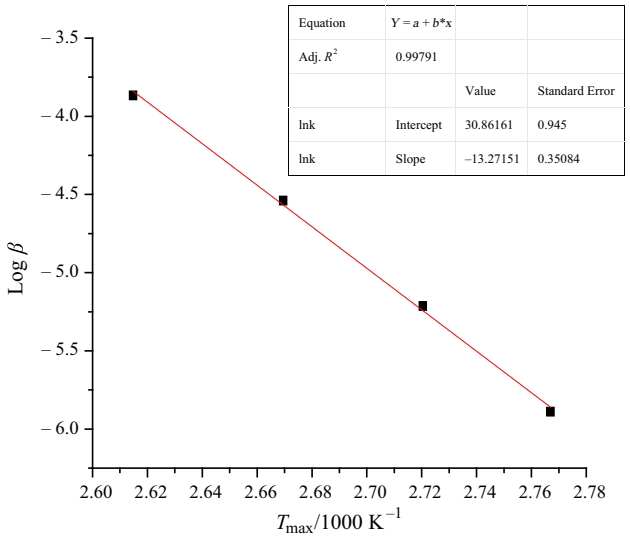

Fig. 5 Evaluation of E_a by ASTM E698-11 method for 98 mass% AIBA at n = 1.0

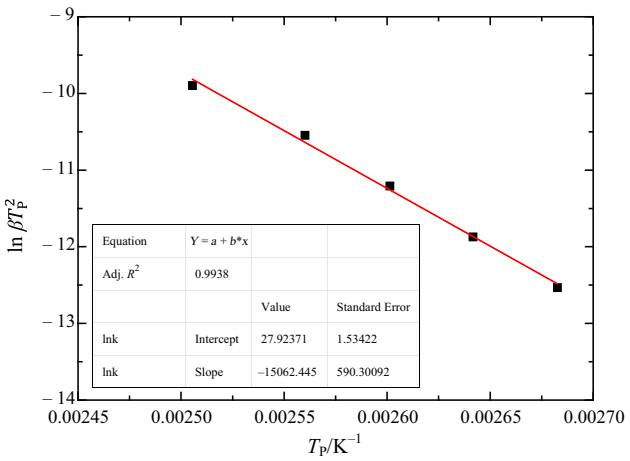

Fig. 6 Evaluation of E_a by Kissinger method for 98 mass% AIBA at n = 1.0

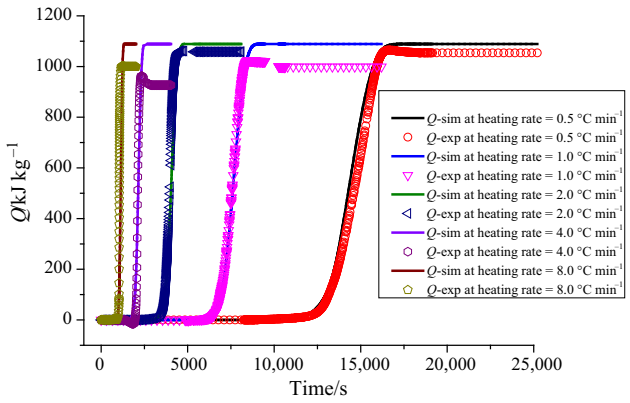

Fig. 7 Comparisons of AIBA heat production versus time curves with heating rates of 0.5, 1.0, 2.0, 4.0, and 8.0 °C min^{-1} by experiments and simulations

showed a reasonable fitting of the DSC data under different heating rates. The formal nth model provides a reasonable fit for the entire set of experimental data. The results produced well-fit curves of heat production rates as shown in Fig. 8. The results closely mirrored the same thermokinetic parameters, such as E_a that were obtained by the nonlinear fitting method, and are also similar to data from the four methods given in Table 1. The schemes of heat production and heat production rate against the time of AIBA reaction at the five heating rates demonstrate that AIBA exhibits complex reaction behavior that the obtained thermokinetic parameters can be used to reliably forecast the thermokinetic parameters using the Semenov model. The related thermokinetic parameters are listed in Table 3.

Calculation mode on process amplification calculation mode

For applying experimental scale of thermal hazard data to the actual process operation, such as design of cooling system or storage and transportation characteristic, we simulated heat generation from large-scale system q_g and external heat release mode q_r based on Eqs. (17) and (18). The parameters to be replaced in the equations are known as fixed values except the T_S. T_S can be substituted into arbitrary value. In general, azos are commonly used at temperature below 90.0 °C. We chose ambient temperature as 323, 333, and 343 K. Adding the conditions of Eqs. (22) and (23), q_g and q_r will have intervals of heat balance ($q_g = q_r$). From the above situations, the curves formed by q_g and q_r have two intersection points defined as the stable point of extinguishing temperature (T_{SE}) and the stable point of initiation temperature (T_{SI}) as well as tangent points defined as critical ignition or extinction

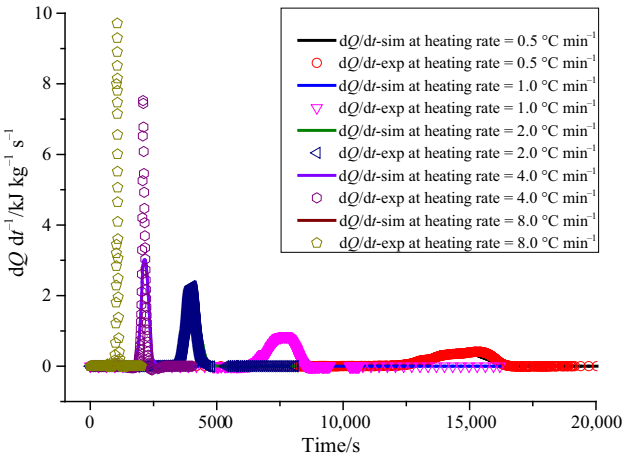

Fig. 8 Comparisons of AIBA heat production rate versus time curves with heating rates of 0.5, 1.0, 2.0, 4.0, and 8.0 °C min^{-1} by experiments and simulations

Table 3 Results of thermokinetic parameters evaluation for the AIBA at 0.5, 1.0, 2.0, 4.0, and 8.0 °C min^{-1}

Parameter	Units	Value
ln (k_0)	ln (s^{-1})	29
E_a	kJ mol^{-1}	130
n	Dimensionless	1
ΔH_d	J g^{-1}	1074

temperature (T_{CI}) and critical extinguishing temperature (T_{CE}), which are shown in Figs. 9–11 with different surrounding temperatures. The numerical method can be beginning from Eq. (25). The two solutions, T_{CE} and T_{CI}, can be attained, and brought to Eq. (19) to obtain two hS values. Finally, different hS is substituted into Eq. (24) for acquiring other critical parameters.

By the tangent and intersection of q_g and q_r, it can determine the AIBA in large scale under different cooling system efficiency (q_{r1}, q_{r2}, and q_{r3}). When the heat q_r is less than or equal to q_{r3}, which means the cooling system efficiency must at least have reached this value. If the temperature exceeds the value represented by the T_{CI}, $q_r < q_g$, the system will tend to be unstable state, or if the temperature exceeds the value of T_{SI}, the $q_r > q_g$, and the system will finally move back to steady state. When the cooling efficiency measures up the q_{r1}, substantially the $q_r \geq q_g$, even if the temperature is greater than T_{SE} and T_{CE}, the system will return to steady state.

From the above description, the ideal state of the cooling system is $q_r \geq q_{r1}$. However, realization of higher cooling

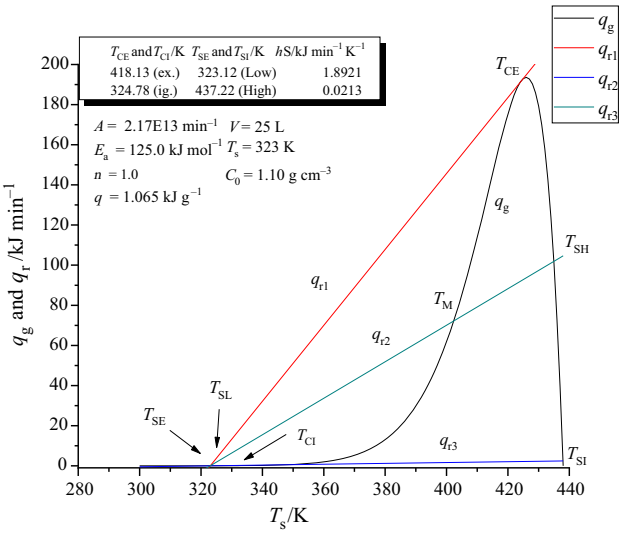

Fig. 9 Balance scheme of heat production rate q_g and heat removal rate q_r for decomposition reaction of 98 mass% AIBA with T_S = 323 K

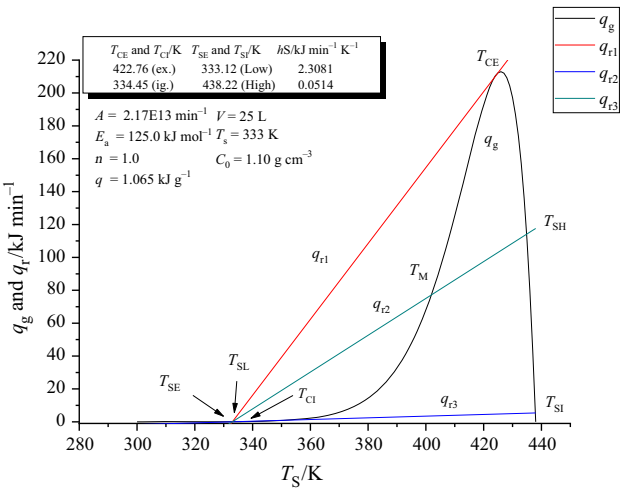

Fig. 10 Balance scheme of heat production rate q_g and heat removal rate q_r for decomposition reaction of 98 mass% AIBA with T_S = 333 K

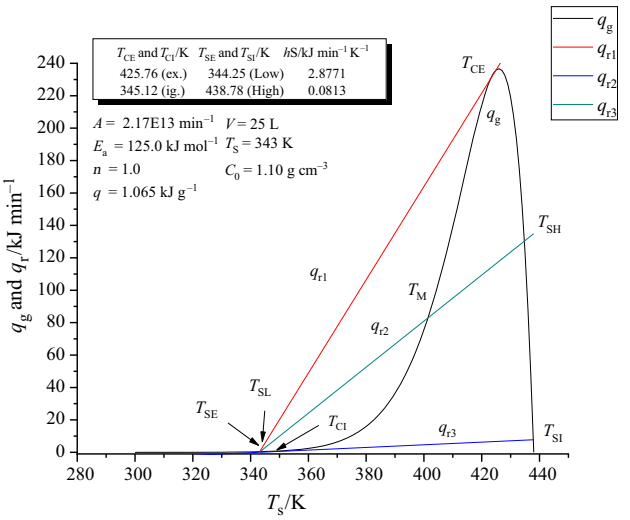

Fig. 11 Balance scheme of heat production rate q_g and heat removal rate q_r for decomposition reaction of 98 mass% AIBA with T_S = 343 K

efficiency often requires costly designs and equipment. Under the compromise, the real process can select a medium cooling system efficiency q_r; there were three intersection points between q_{r3} and q_g, which represents a stable point at lower temperature (T_{SL}), stable point at middle temperature (T_M), and stable point at higher temperature (T_{SH}).

The temperature in a normal operating system should always be maintained below T_M, but when causing an unexpected situation, such as a disoperation or invalid device, the temperature exceeds T_M. If the cooling system does not respond in time, heat accumulation occurs ($q_r < q_g$), and resulting system approaches an unstable state or

runaway reaction. The reaction progresses to T_{SH}, at which point $q_r \geq q_g$ and the system traces back to a steady state.

Conclusions

DSC combined with a mathematical model is a useful method for measuring the thermal hazard of, and avoiding a thermal runaway reaction for, AIBA. Kinetic models can also be integrated with calorimetric data to acquire a variety of thermokinetic parameters. The calculation results can approach more closely to the real situation.

The obtained thermokinetic parameters can be used in the calculation of the process amplification simulation of AIBA under different surrounding temperature during various cooling efficiencies (see Figs. 9–11). When heat discharge rate (hS) is determined by q_{r1} and q_{r3}, T_{CI}, T_{SI}, T_{SE}, and T_{CE} = 324.78, 437.22, 323.12, and 418.13 K (98 mass% AIBA with T_S = 323 K), as the T_S increased on 333 K, T_{CI}, T_{SI}, T_{SE}, and T_{CE} = 334.45, 438.22, 333.12, and 422.76 K. The critical temperature increased when the T_S value was increased. The range of heat transfer coefficients (hS) was 0.0213–2.8771 kJ min^{-1} K^{-1} at 323 K< T_S < 353 K for AIBA.

The decomposition reaction of AIBA analyzed by different DSC heating rates and thermokinetic parameters was constructed from four different kinetic theories. These results were used for predicting the exothermic mode of AIBA at the medium scale (25 L). It will decrease the need for large experiments, which are tedious and expensive. The simulation of thermal behavior can assist in evaluation and design basis for an actual process cooling system, transportation, and storage of AIBA.

Acknowledgements The authors wish to express their gratitude to Dr. Arcady A. Kossoy of ChemInform Saint Petersburg, Federation, Russian, for providing technical assistance. The authors would also like to thank Dr. Shang-Hao Liu and Dr. Kuo-Ming Luo for their help on the measurements of critical parameters.

References

1. United Nations. Recommendations on the transport of dangerous goods: model regulations. 12th Revised ed. New York: United Nations Publications; 2018.
2. Liu SH, Cheng YF, Meng XR, Ma HH, Song SX, Liu WJ, Shen ZW. Influence of particle size polydispersity on coal dust explosibility. J Loss Prev Process Ind. 2018;56:444–50.
3. Dubikhin V, Knerel'man E, Manelis G, Nazin G, Prokudin V, Stashina G, Chukanov N, Shastin A. Thermal decomposition of azobis (isobutyronitrile) in the solid state. Cage effect. Recombination and disproportionation of cyanoisopropyl radicals. Dokl Phys Chem. 2012;446(2):171–5.
4. Gowda S, Abiraj K, Gowda DC. Reductive cleavage of azo compounds catalyzed by commercial zinc dust using ammonium formate or formic acid. Tetrahedron Lett. 2002;43(7):1329–31.
5. Liu SH, Yu YP, Lin YC, Weng SY, Hsieh TF, Hou HY. Complex thermal evaluation for 2,2′-azobis(isobutyronitrile) by non-isothermal and isothermal thermokinetic analysis methods. J Therm Anal Calorim. 2014;116(3):1361–7.
6. Kossoy AA, Belokhvostov VM, Koludarova EY. Thermal decomposition of AIBN: Part D: verification of simulation method for SADT determination based on AIBN benchmark. Thermochim Acta. 2015;621:36–43.
7. Liu SH, Shu CM. Advanced technology of thermal decomposition for AMBN and ABVN by DSC and VSP2. J Therm Anal Calorim. 2015;121(1):533–40.
8. Liu SH, Lin WC, Hou HY, Shu CM. Comprehensive runaway thermokinetic analysis and validation of three azo compounds using calorimetric approach and simulation. J Loss Prev Process Ind. 2017;49:970–82.
9. Berdouzi F, Villemur C, Olivier Maget N, Gabas N. Dynamic simulation for risk analysis: application to an exothermic reaction. Process Saf Environ Prot. 2018;113:149–63.
10. Wu KW, Hou HY, Shu CM. Thermal phenomena studies for dicumyl peroxide at various concentrations by DSC. J Therm Anal Calorim. 2006;83(1):41–4.
11. Shen SJ, Wu SH, Chi JH, Wang YW, Shu CM. Thermal explosion simulation and incompatible reaction of dicumyl peroxide by calorimetric technique. J Therm Anal Calorim. 2010;102(2):569–77.
12. Zhu Y, Chen Y, Zhang L, Li W, Huang B, Wu J. Numerical investigation and dimensional analysis of reaction runaway evaluation for thermal polymerization. Chem Eng Res Des. 2015;104:32–41.
13. Brown ME, Maciejewski M, Vyazovkin S, Nomen R, Sempere J, Burnham A, Opfermann J, Strey R, Anderson HL, Kemmler A, Keuleers R, Janssens J, Desseyn HO, Li CR, Tang TB, Roduit B, Malek J, Mitsuhashi T. Computational aspects of thermokinetic analysis: Part A: the ICTAC thermokinetic project-data, methods and results. Thermochim Acta. 2000;355(1):125–43.
14. Kossoy AA, Benin A, Akhmetshin Y. An advanced approach to reactivity rating. J Hazard Mater. 2005;118(1):9–17.
15. Di Somma I, Andreozzi R, Canterino M, Caprio V, Sanchirico R. Thermal decomposition of cumene hydroperoxide: chemical and thermokinetic characterization. AlChE J. 2008;54(6):1579–84.
16. Chiang CL, Liu SH, Lin YC, Shu CM. Thermal release hazard for the decomposition of cumene hydroperoxide in the presence of incompatibles using differential scanning calorimetry, thermal activity monitor III, and thermal imaging camera. J Therm Anal Calorim. 2017;127(1):1061–9.
17. Wang SY, Kossoy AA, Yao YD, Chen LP, Chen WH. Kinetics-based simulation approach to evaluate thermal hazards of benzaldehyde oxime by DSC tests. Thermochim Acta. 2017;655:319–25.
18. Burnham AK. Computational aspects of thermokinetic analysis Part D: the ICTAC thermokinetic project—multi-thermal-history model-fitting methods and their relation to isoconversional methods. Thermochim Acta. 2000;355(1):165–70.
19. Maciejewski M. Computational aspects of thermokinetic analysis Part B: the ICTAC thermokinetic Project—the decomposition thermokinetic of calcium carbonate revisited, or some tips on survival in the thermokinetic minefield. Thermochim Acta. 2000;355(1):145–54.
20. Roduit B. Computational aspects of thermokinetic analysis Part E: the ICTAC Thermokinetic project—numerical techniques and thermokinetic of solid state processes. Thermochim Acta. 2000;355(1):171–80.
21. Vyazovkin S. Computational aspects of thermokinetic analysis Part C. The ICTAC thermokinetic project—the light at the end of the tunnel. Thermochim Acta. 2000;355(1):155–63.

22. Semenov NN. Thermal theory of combustion and explosion. Washington: National Advisory Committee for Aeronautics; 1942.
23. Talouba IB, Balland L, Mouhab N, Abdelghani-Idrissi M. Thermokinetic parameter estimation for decomposition of organic peroxides by means of DSC measurements. J Loss Prev Process Ind. 2011;24(4):391–6.
24. Liu SH, Lin WC, Xia H, Hou HY, Shu C-M. Combustion of 1-butylimidazolium nitrate via DSC, TG, VSP2, FTIR, and GC/MS: an approach for thermal hazard, property and prediction assessment. Process Saf Environ Prot. 2018;116:603–14.
25. Zhang B, Liu SH, Chi JH. Thermal hazard analysis and thermokinetic calculation of 1,3-dimethylimidazolium nitrate via TG and VSP2. J Therm Anal Calorim. 2018;134:2367–74.
26. Roduit B, Borgeat C, Berger B, Folly P, Andres H, Schädeli U, Vogelsanger B. Up-scaling of DSC data of high energetic materials: simulation of cook-off experiments. J Therm Anal Calorim. 2006;85(1):195–202.
27. Ozawa T. A new method of analyzing thermogravimetric data. Bull Chem Soc Jpn. 1965;38(11):1881–6.
28. Ozawa T. Thermal analysis—review and prospect. Thermochim Acta. 2000;355(1–2):35–42.
29. ASTM. Standard test method for Arrhenius thermokinetic constants for thermally unstable materials. Philadelphia: American Society for Testing and Materials; 1979.
30. Boswell P. On the calculation of activation energies using a modified Kissinger method. J Therm Anal Calorim. 1980;18(2):353–8.
31. Kossoy AA, Hofelich T. Methodology and software for assessing reactivity ratings of chemical systems. Process Saf Prog. 2003;22(4):235–40.
32. Kossoy AA, Sheinman IY. Evaluating thermal explosion hazard by using thermokinetic-based simulation approach. Process Saf Environ Prot. 2004;82(6):421–30.
33. Huang J, Jiang J, Ni L, Zhang W, Shen S, Zou M. Thermal decomposition analysis of 2,2-di-(tert-butylperoxy)butane in non-isothermal condition by DSC and GC/MS. Thermochim Acta 2018. https://www.sciencedirect.com/science/article/pii/S0040603118302326.
34. Filimonov VY, Koshelev KB, Sytnikov AA. Thermal modes of heterogeneous exothermic reactions. Solid-phase interaction. Combust Flame. 2017;185:93–104.
35. Semenov NN. Zur theorie des verbrennungsprozesses. Zeitschrift für Physik. 1928;48(7–8):571–82.
36. Lu G, Zhang C, Chen L, Chen W, Yang T, Zhou Y. Kinetic analysis and self-accelerating decomposition temperature (SADT) of β-nitroso-α-naphthol. Process Saf Environ Prot. 2015;95:69–76.